

## Bifurcation analysis of over-consolidated clays in different stress paths and drainage conditions

De'an Sun<sup>\*1</sup>, Liwen Chen<sup>1</sup>, Junran Zhang<sup>2</sup> and Annan Zhou<sup>3</sup>

<sup>1</sup>Department of Civil Engineering, Shanghai University, Shanghai, 200072, China

<sup>2</sup>Henan Province Key Laboratory of Geotechnical and Structural Engineering, North China University of Water Resources and Electric Power, Zhengzhou, 450045, China

<sup>3</sup>School of Civil, Environmental & Chemical Engineering, RMIT University, Melbourne, 3001, Australia

(Received July 22, 2014, Revised April 27, 2015, Accepted June 20, 2015)

**Abstract.** A three-dimensional elastoplastic constitutive model, also known as a UH model (Yao *et al.* 2009), was developed to describe the stress-strain relationship for normally consolidated and over-consolidated soils. In this paper, an acoustic tensor and discriminator of bifurcation for the UH model are derived for the strain localization of saturated clays under undrained and fully and partially drained conditions. Analytical analysis is performed to illustrate the points of bifurcation for the UH model with different three-dimensional stress paths. Numerical analyses of cubic specimens for the bifurcation of saturated clays under undrained and fully and partially drained conditions are conducted using ABAQUS with the UH model. Analytical and numerical analyses show the similar bifurcation behaviour of overconsolidated clays in three-dimensional stress states and various drainage conditions. The results of analytical and numerical analyses show that (1) the occurrence of bifurcation is dependent on the stress path and drainage condition; and (2) bifurcation can appear in either a strain-hardening or strain-softening regime.

**Keywords:** bifurcation; over-consolidated; constitutive model; undrained condition; partially drained condition; numerical simulation

### 1. Introduction

A number of engineering failures, such as landslides, foundation failures and tunnel collapses, are related to strain localization. A common feature of these failures in geotechnical engineering is that the shear strain is concentrated in a relatively narrow region, and the failure zone is at first initiated from the strain localization zone. The initial failure zone propagates together with the development of the strain localization zone, which leads to the failure of the entire geotechnical structure.

Theoretical studies of strain localization have been conducted over the last several decades by different researchers. Hill (1958) and Drucker (1959) proposed widely used analytical methods that can predict the occurrence of strain localization in single-phase materials. These prediction and analysis methods were further developed and refined by Rudnicki and Rice (1975), Rice (1976), and Bigoni and Hueckel (1991), etc. Recently, material strain localization in the

---

\*Corresponding author, Professor, E-mail: [sundean@shu.edu.cn](mailto:sundean@shu.edu.cn)

three-dimensional stress state has been highlighted by some researchers. For example, Huang *et al.* (2007) applied micro-polar theory to the hypo-plastic constitutive model and then studied the bifurcation characteristics of sand in the three-dimensional stress state. Huang *et al.* (2010) verified that the predictions of bifurcation theory using the non-coaxial elastoplastic constitutive model are reasonable and in agreement with the results of true triaxial tests on sands. Zhang and Schrefler (2001) launched a series of studies on the initiative condition of strain localization in saturated porous media by means of solution uniqueness, bifurcation and variation principle and positiveness of the second-order work density.

In this paper, an acoustic tensor and discriminator of bifurcation are given in an explicit form for the three-dimensional elastoplastic constitutive model (called UH model) proposed by Yao *et al.* (2009) for over-consolidated clays and for the strain localization of saturated clays under undrained and fully and partially drained conditions. Analytical analysis is performed to illustrate the points of bifurcation for the UH model with different three-dimensional stress paths. Numerical analyses of cubic specimens for the bifurcation of saturated clays under undrained and fully and partially drained conditions are conducted using ABAQUS (ABAQUS Inc. 2006) with the UH model. Analytical and numerical analyses show the similar bifurcation behaviour of overconsolidated clays in three-dimensional stress states and various drainage conditions.

## 2. Three-dimensional constitutive model for over-consolidated clays

The pre-consolidation pressure of over-consolidated clays is greater than the current consolidation pressure; thus, their mechanical behaviour is different from that of normally consolidated (NC) clays. Naturally deposited clays are often found in different over-consolidated states. Compared with normally consolidated clays, over-consolidated (OC) clays have a lower void ratio and higher strength and exhibit more complicated behaviours, such as shear dilatancy and strain-softening. Therefore, the strain localization characteristics of over-consolidated clays and normally consolidated clays are different. The formation and development of strain localization during loading are largely dependent on the elastoplastic matrix of the constitutive model. To reflect the formation and development process of the strain localization of over-consolidated clays, a reasonable constitutive model is needed to describe the mechanical behaviour.

In this paper, to investigate the strain localization of over-consolidated clays, an elastoplastic constitutive model called the UH model (Yao *et al.* 2009) is employed. The model is generalised to a three-dimensional model in which the Matsuoka-Nakai criterion is adopted using the transformed stress method (Matsuoka *et al.* 1999). The model can capture the stress-path-dependent stress-strain relationship, shear dilatancy, strain hardening and softening of over-consolidated clays in three-dimensional stress states. The yield function is written as

$$f = \frac{\lambda - \kappa}{1 + e_0} \left[ \ln \frac{\tilde{p}}{\tilde{p}_0} + \ln \left( 1 + \frac{\tilde{q}^2}{M^2 \tilde{p}^2} \right) \right] - \tilde{H} = 0 \quad (1)$$

where  $\lambda$  and  $\kappa$  are the slopes of the normal compression curve and unloading line, respectively,  $e_0$  is the initial void ratio, the superscript  $\sim$  denotes transformed stress,  $p$  and  $q$  are the mean and deviatoric stresses, respectively,  $M$  is the stress ratio ( $q/p$ ) at the critical state,  $\tilde{p}_0$  is a constant that corresponds to the length of the  $p$ -axes of the reference yield ellipses at an initial condition when

the plastic volumetric strain  $\varepsilon_v^p = 0$ . In addition,  $H$  is a hardening parameter expressed by

$$H = \int dH = \int \frac{M_f^4 - \tilde{\eta}^4}{M^4 - \tilde{\eta}^4} d\varepsilon_v^p \tag{2}$$

in which  $\tilde{\eta} = \tilde{q} / \tilde{p}$  is the stress ratio in transformed stress space and  $M_f$  is the stress ratio ( $\tilde{q} / \tilde{p}$ ) at the potential peak failure. To express the peak strength of over-consolidated clays, an improved Hvorslev envelope is adopted using a parabolic curve (Yao *et al.* 2012).  $M_f$  is written as

$$M_f = 6 \left[ \sqrt{\frac{k_1}{R} \left( 1 + \frac{k_1}{R} \right)} - \frac{k_1}{R} \right] \tag{3}$$

with

$$R = \frac{\tilde{p}_0}{\tilde{p}_0} \left( 1 + \frac{\tilde{\eta}^2}{M^2} \right) \exp \left( -\frac{1 + e_0}{\lambda - \kappa} \varepsilon_v^p \right) \quad 0 < R \leq 1 \tag{4}$$

and

$$k_1 = \frac{M^2}{12(3 - M)} \tag{5}$$

where  $R$  is an over-consolidation parameter, and  $\tilde{p}_0$  corresponds to the pre-consolidation pressure.

### 3. Localised bifurcation analyses

#### 3.1 Bifurcation criterion

The bifurcation was resolved by the acoustic tensor method proposed by Rudnicki and Rice (1975). It was assumed that the velocity and stress fields are continuous up to a state at which the planar weak discontinuities may develop in a homogeneous specimen under uniform deformation. Across a weak discontinuity plane  $S$ , as shown in Fig. 1, the velocity and stress fields are initially continuous, but the gradient of the velocity field experiences a jump that can be expressed by

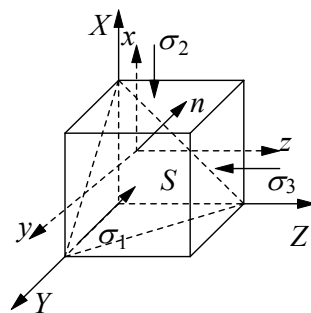


Fig. 1 Sketch of weak discontinuity plane in principal stress space

$$[[v_{i,j}]] = v_{i,j}^i - v_{i,j}^o = g_i n_j; \quad [[v_i]] = v_i^i - v_i^o = 0 \quad (6)$$

where  $[[ \ ]]$  denotes the jump of a variable,  $v_i$  is the velocity, superscripts  $i$  and  $o$  denote being within and outside a band, respectively,  $v_{i,j} = \partial v_i / \partial x_j$  is the velocity gradient,  $g_i$  is a jump size measure of a variable across the strain localization zone, and  $n_j$  is the normal direction to the zone. From

$$\left. \begin{aligned} \varepsilon_{ij} &= \frac{1}{2}(u_{i,j} + u_{j,i}) \\ u_i &= v_i dt \end{aligned} \right\} \quad (7)$$

we have

$$\dot{\varepsilon}_{ij} = \frac{1}{2}(u_{i,j} + u_{j,i}) \quad (8)$$

Then, the jump of the velocity gradient field is produced

$$[[\dot{\varepsilon}_{ij}]] = \frac{1}{2}(g_i n_j + g_j n_i) \quad (9)$$

where  $\varepsilon_{ij}$  and  $\dot{\varepsilon}_{ij}$  are the strain tensor and strain rate tensor, respectively, and  $u_i$  is the displacement vector.

The governing equations for consolidation problems of saturated soils can be expressed as follows

$$\left. \begin{aligned} \sigma_{ij,j}'' + p_{w,i} &= 0 \\ \dot{w}_i + k p_{w,i} &= 0 \\ Q(\dot{w}_{i,i} - \dot{u}_{i,i}) + \dot{p}_w &= 0 \end{aligned} \right\} \quad (10)$$

where  $\sigma_{ij}'' = \sigma_{ij} - \delta_{ij} p_w$  is the effective stress ( $\delta_{ij}$  is Kronecker's delta),  $\sigma_{ij}$  is the total stress,  $u_i$  is the displacement of the soil skeleton,  $w_i$  is the average velocity of the pore water relative to the soil skeleton,  $p_w$  is the pore water pressure,  $k$  is the coefficient of permeability, and the parameter  $Q$  is defined as

$$Q = \left[ \frac{n}{K_w} + \frac{1-n}{K_s} \right]^{-1} \quad (11)$$

where  $K_s$  and  $K_w$  are the bulk moduli of soil particles and pore-water, respectively, and  $n$  is porosity. In general,  $K_s \gg K_w$  gives  $Q \approx (n / K_w)^{-1}$ .

From Eq. (10), the equation for drainage state is written as follows (Zhang and Schrefler 2001)

$$\left[ \left( D_{ijkl} + \frac{1}{\zeta} Q_{ijkl} \right) \dot{\varepsilon}_{kl} \right]_{,i} = 0 \quad (12)$$

where

$$\left. \begin{aligned} Q_{ijkl} &= Q\delta_{ij}\delta_{kl} \\ \zeta &= 1 + \frac{Qk}{r} \\ r &= \frac{-\omega}{K_1^2 + K_2^2 + K_3^2} \end{aligned} \right\} \quad (13)$$

in which  $k$ ,  $\omega$ ,  $K_1$ ,  $K_2$  and  $K_3$  are parameters.  
 Substituting Eq. (9) into Eq. (12) leads to

$$n_i \left( D_{ijkl} + \frac{1}{\zeta} Q_{ijkl} \right) n_k g_l = 0 \quad (14)$$

When the bifurcation occurs, then  $g_l \neq 0$  and the bifurcation criterion for the drainage conditions is written as follows

$$\det(\xi_{jl}) = \det \left( n_i \left( D_{ijkl} + \frac{1}{\zeta} Q_{ijkl} \right) n_k \right) = 0 \quad (15)$$

where **det** denotes the determinant.

When  $\zeta \rightarrow +\infty$ , Eq. (15) reduces to the bifurcation criterion for saturated soils under fully drained conditions and can be written as follows

$$\det(\xi_{jl}) = \det(n_i D_{ijkl} n_k) = 0 \quad (16)$$

When  $k = 0$  or  $\zeta = 1$ , Eq. (15) reduces to the bifurcation criterion for saturated soils under undrained conditions and can be written as follows (Zhang and Schrefler 2001)

$$\det(\xi_{jl}) = \det(n_i (D_{ijkl} + Q_{ijkl}) n_k) = 0 \quad (17)$$

where  $\xi_{ij}$  is the acoustic tensor,  $n_i$  is the unit vector normal to the strain localization band, and  $D_{ijkl}$  is an elastoplastic constitutive tensor.

### 3.2 Analytical expression of bifurcation

Results from true triaxial tests on soil materials by Matsuoka and Nakai (1976) show that the failure plane in soil specimens is generally perpendicular to the intermediate principal stress plane. Therefore, we assume that the normal direction of the shear band plane under three-dimensional principal stress conditions is perpendicular to the direction of the intermediate principal stress. Thus, the shear zone is along the direction of the intermediate principal stress. However, the value of the intermediate principal stress affects the bifurcation condition. Substituting  $n_2 = 0$  into Eqs. (15)-(17), the bifurcation condition is obtained as follows

$$A \tan^4 \theta + B \tan^2 \theta + C = 0 \quad (18)$$

with

$$\tan \theta = \frac{n_1}{n_3} \quad (19)$$

in which  $\theta$  is the incline angle of the normal direction of the shear zone,  $n_1$  and  $n_3$  are the cosines of the normal direction of the shear zone. If only the soil skeleton phase (saturated soils under fully drained conditions) is considered, the bifurcation condition is

$$\left. \begin{aligned} A &= D_{1313}D_{1111} \\ B &= D_{1111}D_{3333} - D_{1133}D_{1313} - D_{3311}D_{1313} - D_{1133}D_{3311} \\ C &= D_{1313}D_{3333} \end{aligned} \right\} \quad (20)$$

For saturated soils under undrained conditions, the bifurcation condition is given as follows

$$\left. \begin{aligned} A &= D_{1313}(D_{1111} + Q) \\ B &= D_{1111}D_{3333} - D_{1133}D_{1313} - D_{3311}D_{1313} - D_{1133}D_{3311} + \\ &\quad Q(D_{1111} + D_{3333} - D_{1133} - D_{1313} - 2D_{1313}) \\ C &= D_{1313}(D_{3333} + Q) \end{aligned} \right\} \quad (21)$$

For saturated soils under partially drained conditions, the bifurcation condition is listed as follows

$$\left. \begin{aligned} A &= D_{1313}\left(D_{1111} + \frac{1}{\zeta}Q\right) \\ B &= D_{1111}D_{3333} - D_{1133}D_{1313} - D_{3311}D_{1313} - D_{1133}D_{3311} + \\ &\quad \frac{1}{\zeta}Q(D_{1111} + D_{3333} - D_{1133} - D_{1313} - 2D_{1313}) \\ C &= D_{1313}\left(D_{3333} + \frac{1}{\zeta}Q\right) \end{aligned} \right\} \quad (22)$$

where  $D_{ijkl}$  denotes the stiffness tensor.

The bifurcation stress point will occur if Eq. (18) has a real solution. The criterion of the real solution is shown as follows

$$Y = \frac{B}{A} \leq 0, \quad Z = B^2 - 4AC \geq 0 \quad (23)$$

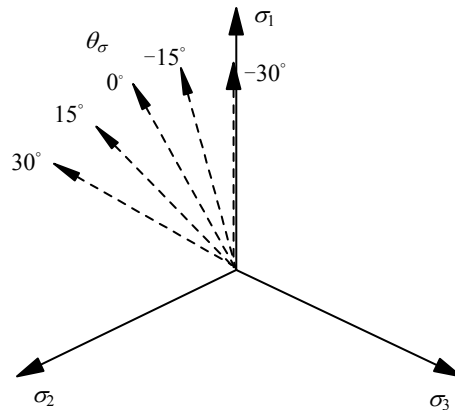
Then, the incline angle of the normal direction of the shear zone is given as follows

$$\theta = \pm \arctan\left(\sqrt{\frac{-B}{2A}}\right) \quad (24)$$

When the UH model (Yao *et al.* 2009) is employed, the elasto-plastic constitutive tensor  $D_{ijkl}$  is listed in Appendix.

Table 1 UH model parameters for Fujinomori clay

$e_0$	$\lambda/(1+e_0)$	$\kappa/(1+e_0)$	$M$	$\nu$
1.0	0.0508	0.0112	1.36	0.3


 Fig. 2 Stress paths for bifurcation analysis in the  $\pi$ -plane

Based on the bifurcation solutions of the three-dimensional constitutive model for over-consolidated and saturated clays under undrained and fully and partially drained conditions, the following theoretical bifurcation solution of the model is achieved for Fujinomori clay with a constant total minor principal stress ( $\sigma_3 = 200$  kPa) and an initial over-consolidation ratio OCR = 8. The material parameters for the model are the same as those in the Cam-clay model, as listed in Table 1. The values in Table 1 are from Matsuoka *et al.* (1999). Here  $\lambda$  and  $\kappa$  are the slopes of normal compression line and unloading line,  $M$  is the slope of critical state line and  $e_0$  is an initial void ratio. Using the parameter values in Table 1, Yao *et al.* (2009) showed that the UH model can describe the mechanical behaviour of overconsolidated Fujinomori clay, including the dilatancy characteristics and hardening-softening behaviour.

Fig. 2 shows the stress path in the  $\pi$ -plane stress with Lode angles  $\theta_\sigma$  of  $\pm 15^\circ$ ,  $0^\circ$  and  $\pm 30^\circ$ . The calculation of bifurcation was conducted under a constant total minor principal stress ( $\sigma_3 = 200$  kPa) condition, along the different stress paths, as shown in Fig. 2. Therefore, the following relations are satisfied.

$$\sigma_3 = 200 \text{ kPa}; \quad \frac{2\sigma_2 - \sigma_1 - \sigma_3}{\sigma_1 - \sigma_3} = \sqrt{3} \tan \theta_\sigma \quad (25)$$

Combining Eq. (18) with Eq. (25) leads to the bifurcation solutions corresponding to different Lode angles under the minor principal stress of 200 kPa.

### 3.3 Analytical result of bifurcation

#### (1) Saturated clays under fully drained conditions

Fig. 3 shows the stress-strain relations and bifurcation solutions along different three-dimensional stress paths for saturated clays under fully drained conditions. In Fig. 3, the

relationships between the stress ratio, volumetric strain and major principal strain are calculated using the constitutive model for over-consolidated clays.

Fig. 3(a) shows that, when the Lode angle is  $-30^\circ$ , which corresponds to the conventional triaxial compression stress state, solving Eqs. (18) and (25) jointly reveals that the function  $Z$  in Eq. (23) is always less than 0. Namely, Eq. (18) has no real solution in the conventional triaxial compression stress state. Therefore, there is no bifurcation during loading along the conventional triaxial compression stress path.

Figs. 3(b) and (c) show the analytical bifurcation solutions when the Lode angle is  $-15^\circ$  and  $0^\circ$ , respectively. When the major principal strain  $\varepsilon_1 > 5.18\%$  and  $6.33\%$ , respectively, the real solutions of Eq. (18) can be obtained,  $Y < 0$  and  $Z > 0$ . The major principal strains  $\varepsilon_1 = 5.18\%$  and  $6.33\%$  are the bifurcation points along the stress path for Lode angles of  $-15^\circ$  and  $0^\circ$ , and the

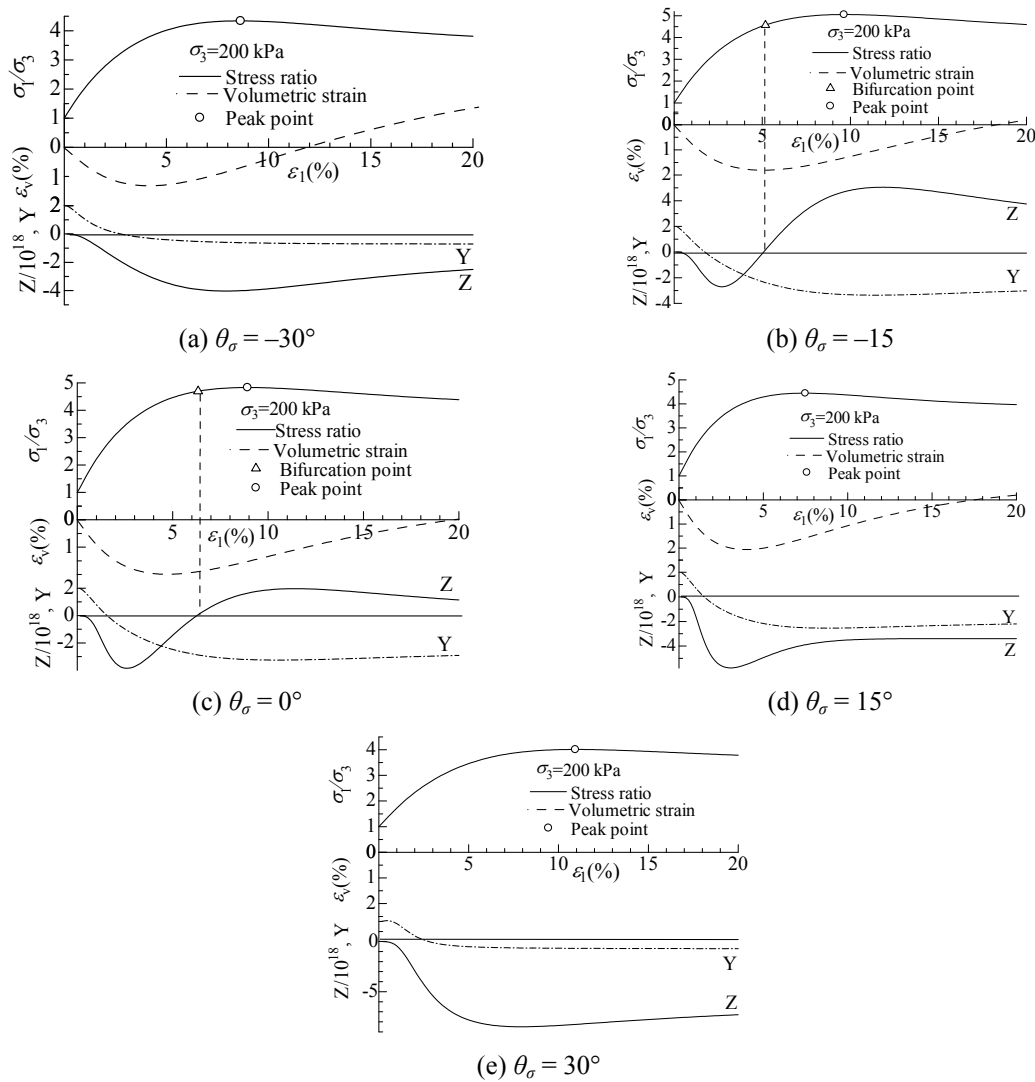


Fig. 3 Analytical bifurcation solutions for soil skeleton along different three-dimensional stress paths

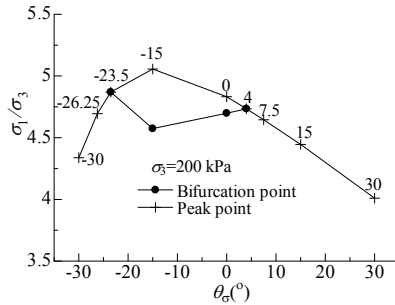


Fig. 4 Stress ratios at bifurcation and peak for different Lode angles for saturated clays under fully drained conditions

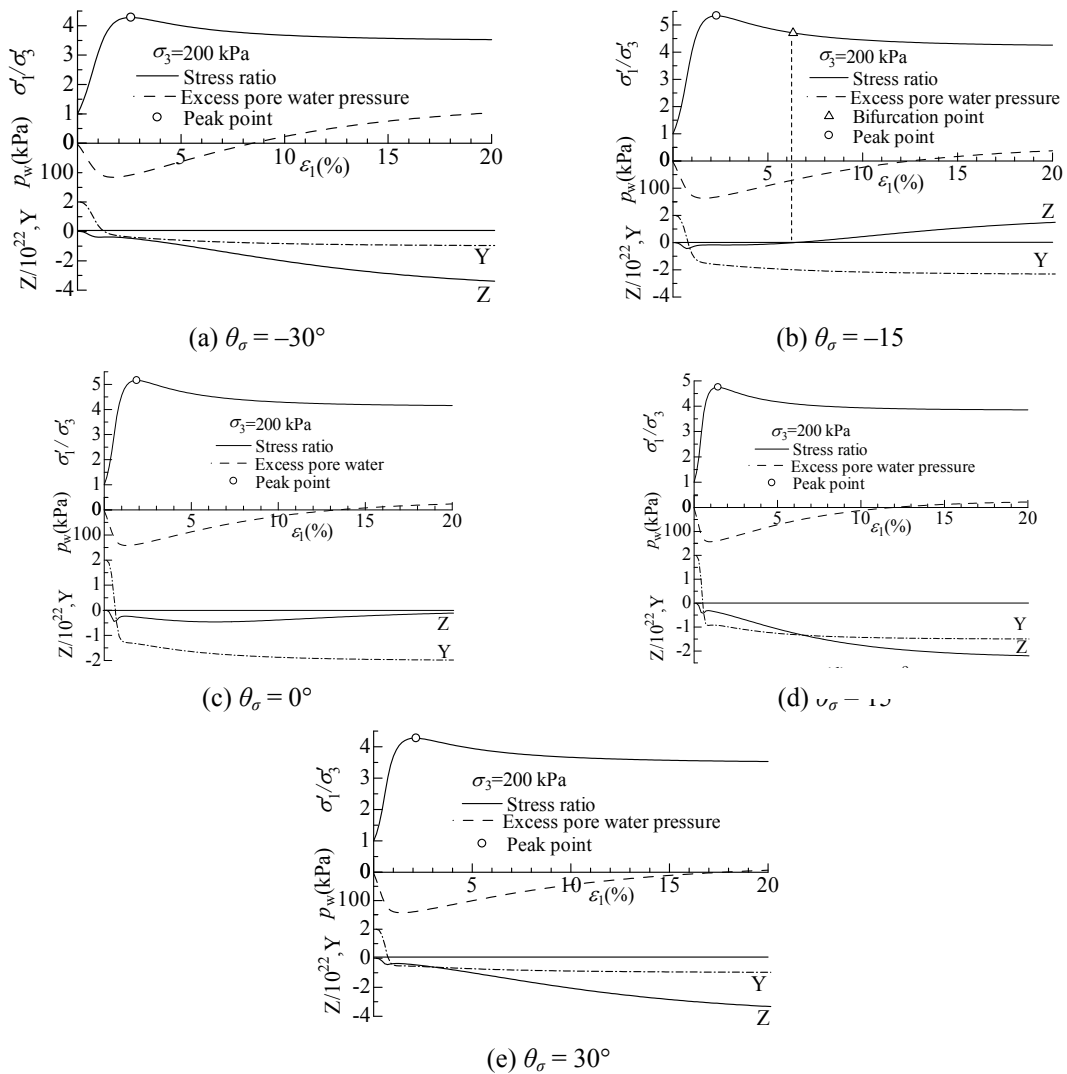


Fig. 5 Analytical bifurcation solutions for saturated clays along different stress paths under undrained conditions

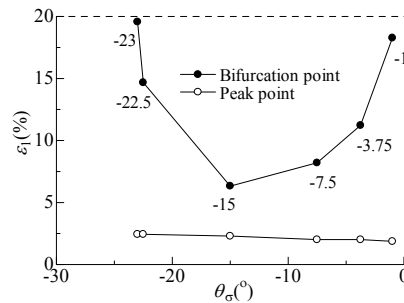


Fig. 6 Major principal strains at bifurcation and peak along different stress paths for saturated clays under undrained conditions

points of bifurcation are located at the hardening regime of the stress-strain relationships of over-consolidated clays.

Figs. 3(d) and (e) are similar to Fig. 3(a). Along the stress paths for Lode angles of  $15^\circ$  and  $30^\circ$ , which correspond to the triaxial extension stress state, Eq. (18) does not have any real solutions because its discriminant  $Z$  is negative, i.e.,  $Z < 0$ , which indicates that there is no bifurcation along these two stress paths.

Fig. 4 shows the relationship between the stress ratios at peak and bifurcation and the Lode angle for saturated clays under fully drained conditions when the minor principal stress  $\sigma_3 = 200$  kPa. The figure shows that onset of bifurcation occurs in the hardening regime of Lode angles between  $-23.5^\circ$  and  $4^\circ$ , and there is no bifurcation in the Lode angle ranges of  $-30^\circ \sim -23.5^\circ$  or  $4^\circ \sim 30^\circ$ .

### (2) Saturated clays under undrained conditions

Fig. 5 shows the stress-strain relationships with bifurcation solutions along different three-dimensional stress path for saturated clays under undrained conditions. Fig. 5(a) shows that, when the Lode angle is  $-30^\circ$ , the discriminant  $Z$  of Eq. (18) is always less than 0. Namely, the equation has no real solutions. Thus, there is no bifurcation for saturated clays in the stress state of conventional triaxial compression and under undrained conditions. Fig. 5 (b) shows the analytical bifurcation solutions at a Lode angle of  $-15^\circ$ . When  $\epsilon_1 > 6.33\%$ , there is a real solution of Eq. (18), i.e.,  $Y < 0$  and  $Z > 0$ ; thus, the major principal strain  $\epsilon_1 = 6.33\%$  is a bifurcation point along the stress path for a Lode angle of  $-15^\circ$ , and the point of bifurcation is at the strain-softening regime of the stress-strain relationships. Figs. 5(c), (d) and (e) are similar to Fig. 5(a); the function  $Z$  in Eq. (23) is always less than 0, which means that Eq. (18) has no real solutions. Thus, there is no bifurcation along the stress path for Lode angles of  $0^\circ$ ,  $15^\circ$  or  $30^\circ$ .

Fig. 6 shows the relationship between the Lode angle and major principal strains corresponding to the bifurcation and the peak of the stress-strain curve for saturated clays when  $\sigma_3 = 200$  kPa and under undrained conditions. The figure shows that there is bifurcation in the Lode angle range of  $-23^\circ \sim -1^\circ$ . All strains at peak are less than the strains corresponding to bifurcation, which means that bifurcation occurs in the strain-softening regime of Lode angles between  $-23^\circ$  and  $-1^\circ$ . There is no bifurcation in the Lode angle ranges of  $-30^\circ \sim -23^\circ$  or  $-1^\circ \sim 30^\circ$ .

### (3) Saturated clays under partially drained conditions

Fig. 7 shows the analytical bifurcation solution along different three-dimensional stress paths.  $\zeta$

is a parameter related to the coefficient of permeability, the bulk modulus of pore-water, and the eigenvalues of Eq. (10), as shown in Eq. (13). For details, see Zhang and Schrefler (2001).  $\zeta = 1$  and  $1 < \zeta < +\infty$  correspond to the analytical bifurcation solutions of saturated clays under undrained and partially drained conditions, respectively, while  $\zeta \rightarrow +\infty$  corresponds to the analytical bifurcation solution of saturated clays under fully drained conditions.

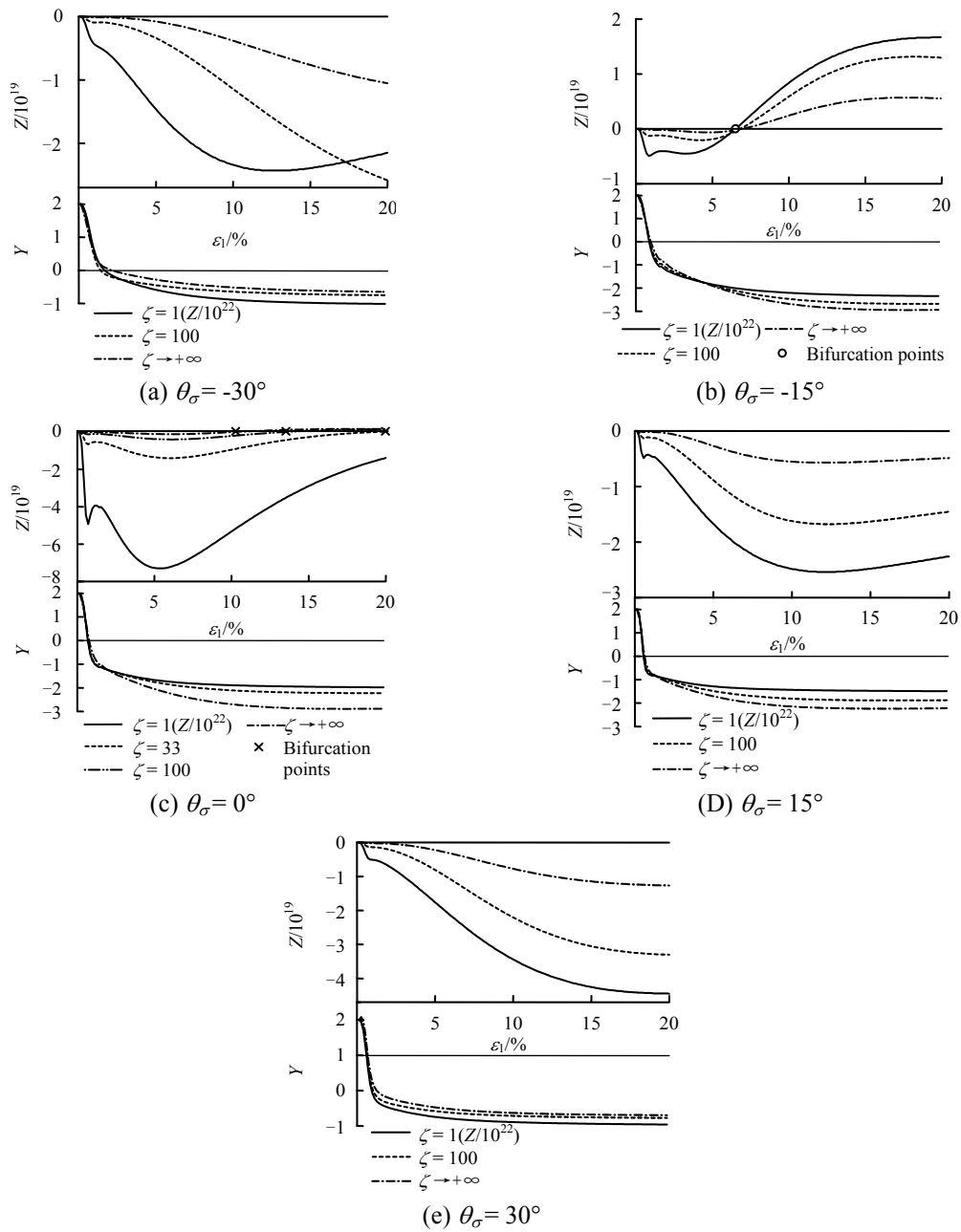


Fig. 7 Analytical bifurcation solutions along different three-dimensional stress paths ( $\sigma_3 = 200$  kPa)

Fig. 7(a) shows the result of the bifurcation analysis for Lode angle of  $30^\circ$ , the triaxial compression state. When  $\zeta$  is in the range  $[1, +\infty)$ , Eq. (18) has no real solutions; thus, the function  $Z$  in Eq. (23) is always less than 0, which indicates that there is no bifurcation at the triaxial compression stress state for saturated clays under undrained and fully and partially drained conditions. Fig. 7(b) shows the analytical bifurcation solution for a Lode angle of  $-15^\circ$ . When  $\zeta$  is in the range  $[1, +\infty)$ , if  $\varepsilon_1 > 6.5\%$ , there is a real solution to Eq. (18), and  $Y < 0$  and  $Z > 0$  in Eq. (23) are satisfied. Hence, the major principal strain of 6.5% is a bifurcation point at  $\theta_\sigma = -15^\circ$  for saturated clays under partially drained conditions. The major strains at bifurcation points under different values of  $\zeta$  are almost the same. Fig. 7(c) shows the analytical bifurcation solution at a Lode angle of  $0^\circ$ . When  $1 \leq \zeta < 33$ , the function  $Z$  in Eq. (23) is always less than 0; thus, the Eq. (18) has no real solutions, which indicates there is no bifurcation point during loading along this stress path. When  $33 \leq \zeta < +\infty$ , if  $\varepsilon_1$  equals a value within the range specified in Eq. (23),  $Y < 0$  and  $Z > 0$ , and Eq. (18) has real solutions, indicating the existence of a bifurcation. With increasing  $\zeta$ , the bifurcation point moves forward.

Figs. 7(d) and (e) show the analytical bifurcation solutions for Lode angles of  $15^\circ$  and  $30^\circ$ , respectively. The figures show that the function  $Z$  in Eq. (23) is always less than 0, which indicates that there is no bifurcation along the stress paths for Lode angles of  $15^\circ$  and  $30^\circ$  (corresponding to the triaxial extension stress state) for saturated clays under undrained and partially and fully drained conditions.

## 4. Numerical simulations of true triaxial tests for identifying bifurcation

### 4.1 Conditions of numerical simulations

To verify the validity of the analytical solutions, numerical analyses were performed to detect the strain localization of saturated over-consolidated clay under undrained and fully and partially drained conditions. A subroutine code of the three-dimensional constitutive model for over-consolidated clays based on the improved Hvorslev envelope was implemented with the finite element software ABAQUS. The object of this analysis was a homogeneous and isotropic cube with side lengths of 10 cm. An 8-node hexahedral linear element was employed. The cube was divided into  $14 \times 14 \times 14 = 2744$  units; the finite element meshes are shown in Fig. 8.

The vertical direction is set to the major principal stress direction, and the other two horizontal directions are the intermediate and minor principal stress directions. The top and bottom surfaces

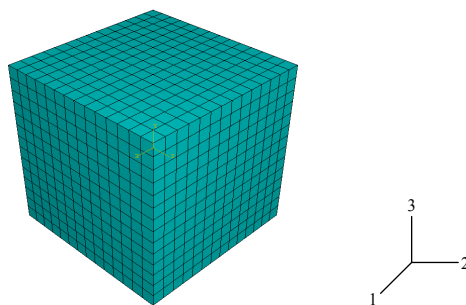


Fig. 8 Meshes for finite element analysis

are set to be perfectly smooth. The forced vertical displacements were imposed down on the top surface. Also, the vertical displacements on the bottom surface are fixed. Saturated soil used units adopted by the C3D8P in ABAQUS. For undrained conditions, there is no drainage boundary, while the drainage boundary was set on the top surface under partially drainage conditions. A fixed time increment of 0.001 day was adopted for each step, and the total computing time was set to be 0.139 days for achieving the major principal strain of 20%. When the computation stops on the computing way the point is considered to be the bifurcation. The initial over-consolidation ratio of the specimen is assumed to be 8, and the constitutive model parameters are listed in Table 1.

4.2 Results of numerical simulation

Fig. 9 shows the numerical solutions of the stress-strain relationship up to the bifurcation along

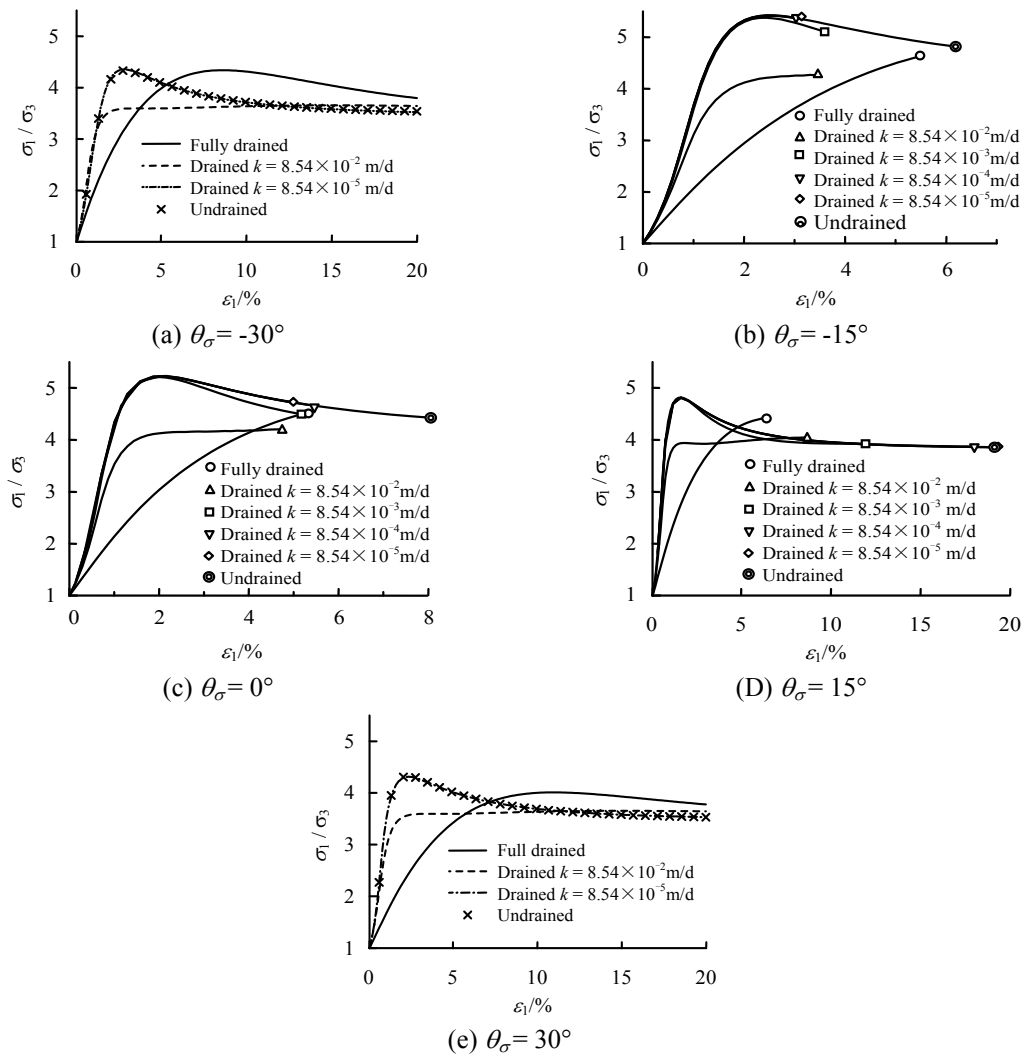


Fig. 9 Numerical solutions up to bifurcation along different three-dimensional stress paths ( $\sigma_3 = 200$  kPa)

different three-dimensional stress paths. The stress and strain are the average of the whole structure in Fig. 8. Figs. 9(a) and (e) show that when the Lode angle is  $-30^\circ$  or  $30^\circ$ , there is no bifurcation for saturated clays under undrained and fully and partially drained conditions. Last plots in Figs. 9(b), (c) and (d) denote the bifurcation points. Fig. 9(b) shows that there are bifurcations at a Lode angle of  $-15^\circ$  for saturated clays under undrained and fully and partially drained conditions, with the bifurcation point being the principal strain, ranging from 3.0% to 6.2%. Similar to Fig. 9(b), Fig. 9(c) shows that when the Lode angle is  $0^\circ$ , the bifurcations occur at the major principal strain, ranging from 4.5% to 8.6%.

Fig. 9(d) shows that when the Lode angle is  $15^\circ$ , the bifurcation of saturated clay under fully drained conditions appears the earliest, with major principal strain of 6.3%. For saturated clays under partially drained conditions, a small permeability coefficient  $k$  means that bifurcation appears later. When  $k = 8.54 \times 10^{-5}$  m/d, the major principal strain corresponding to the bifurcation is 19.42%. Under undrained conditions, the major principal strain corresponding to the bifurcation is 19.14%. As shown in Fig. 9(b), (c) and (c), the bifurcation appears in the strain-hardening regime of the stress-strain curve for saturated clays under fully drained conditions, while the bifurcation appears in the strain-softening regime of the stress-strain curve for saturated clays.

#### 4.3 Comparison of numerical simulation and analytical solution

Table 2 summarises the results of analytical and numerical bifurcation solutions for saturated over-consolidated clays under undrained and fully and partially drained conditions along different

Table 2 Bifurcation points by analytical and numerical analyses

		$\theta_\sigma$ ( $^\circ$ )					
		-30	-15	0	15	30	
Saturated clay under fully drained conditions	Analytical	Not bifurcated	Bifurcated (5.18%)	Bifurcated (6.33%)	Not bifurcated	Not bifurcated	
	Numerical	Not bifurcated	Bifurcated (5.5%)	Bifurcated (5.3%)	Bifurcated (6.3%)	Not bifurcated	
Saturated clays	Partially drained conditions	Analytical	Not bifurcated	Bifurcated (6.5%) (unrelated to $\zeta$ )	Bifurcated (critical point $\zeta=33$ ) (related to $\zeta$ )	Not bifurcated	Not bifurcated
	Numerical	Not bifurcated	Bifurcated (3.0%~3.6%) (unrelated to $k$ )	Bifurcated (4.7%~5.5%) (unrelated to $k$ )	Bifurcated (8.6%~19.42%) ( $k$ larger, bifurcation appear earlier)	Not bifurcated	
Undrained conditions	Analytical	Not bifurcated	Bifurcated (6.33%)	Not bifurcated	Not bifurcated	Not bifurcated	
	Numerical	Not bifurcated	Bifurcated (6.2%)	Bifurcated (8.1%)	Bifurcated (19.1%)	Not bifurcated	

Note: ( ) represents the value of major principal strain at bifurcation points

three-dimensional stress paths. The values in brackets (such as 5.5%) in the table represent major principal strains at which bifurcation occurs. As shown in Table 2, when the Lode angle is  $-30^\circ$  or  $30^\circ$ , the analytical and numerical solutions are not bifurcated. When the Lode angle is  $-15^\circ$ , both the analytical and numerical solutions are bifurcated. Under partially drained condition, from the analytical results the bifurcation always takes place regardless of  $\zeta$  value (Fig. 7(b)), and from the numerical results the bifurcation takes place regardless of  $k$  value (Fig. 9(b)). When the Lode angle is  $0^\circ$ , the analytical bifurcation solution occurs for saturated clay under fully drained conditions but does not occur for saturated clays under undrained conditions, while the occurrence of bifurcations depends on the parameter  $\zeta$  under partially drained conditions. When the Lode angle is  $15^\circ$ , bifurcation occurred in the analytical and numerical solutions. For saturated clays under partially drained conditions, a large permeability coefficient  $k$  resulted in an early appearance of bifurcation. The bifurcation predicted by the numerical solution is more likely to occur than that by analytical solutions along the same stress paths because the pore water pressure and effective stress distribution from numerical simulation are not uniform in the specimens, which causes the stress path in some units to deviate from the original stress path, culminating in bifurcation.

## 5. Conclusions

Based on a three-dimensional elastoplastic constitutive model for over-consolidated clays, an acoustic tensor and discriminator of the bifurcation for strain localization of saturated clays under undrained and fully and partially drained conditions are given explicitly. The theoretical analysis shows that, for saturated clays under fully drained conditions, bifurcation occurs in the strain-hardening regime for Lode angles between  $-23.5^\circ$  and  $4^\circ$ , while no bifurcation occurs at Lode angles in the ranges of  $-30^\circ \sim -23.5^\circ$  and  $4^\circ \sim 30^\circ$ . However, for saturated clays under undrained conditions, bifurcation occurs in the strain-softening regime for Lode angles in the range of  $-23^\circ \sim -1^\circ$ , while no bifurcation occurs at Lode angles in the ranges of  $-30^\circ \sim -23^\circ$  and  $-1^\circ \sim 30^\circ$ . Numerical analyses of cubic specimens for the bifurcation of saturated over-consolidated clays under undrained and fully and partially drained conditions are conducted using ABAQUS with the UH model, which shows the similar bifurcation behaviour obtained from analytical analyses for overconsolidated clays in three-dimensional stress states and various drainage conditions.

## References

- ABAQUS Inc. (2006), ABAQUS user's and theory manuals, Version 6.6; Providence Rhode Island.
- Bigoni, D. and Hueckel, T. (1991), "Uniqueness and localization-I associative and non-associative elasto-plasticity", *Int. J. Solid. Struct.*, **28**(2), 197-213.
- Drucker, D.C. (1959), "A definition of stable inelastic materials", *J. Appl. Mech.*, **26**(1), 101-106.
- Hill, R. (1958), "A general theory of uniqueness and stability in elastic-plastic solids", *J. Mech. Phys. Solid.*, **6**(3), 236-249.
- Huang, W.X., Sun, D.A. and Sloan, S.W. (2007), "Analysis of the failure mode and softening behaviour of sands in true triaxial tests", *Int. J. Solid. Struct.*, **44**(5), 1423-1437.
- Huang, M.S., Lv, X.L. and Qian, J.G. (2010), "Non-coaxial elasto-plasticity model and bifurcation prediction of shear banding in sands", *Int. J. Numer. Anal. Method. Geomech.*, **34**(9), 906-919.
- Matsuoka, H. and Nakai, T. (1974), "Stress-deformation and strength characteristics of soil under three difference principal stresses", *Proc. JSCE*, **232**, 59-70.

- Matsuoka, H. and Nakai, T. (1976), "Closure to discussion on "Stress-deformation and strength characteristics of soil under three-different principal stress", *Proc. JSCE*, **246**, 139-140. [In Japanese]
- Matsuoka, H., Yao, Y.P. and Sun, D.A. (1999), "The Cam-clay model revised by the SMP criterion", *Soil. Found.*, **39**(1), 81-95.
- Rice, J.R. (1976), *The Localization of Plastic Deformation, Theoretical and Applied Mechanics*, (Koiter, W.T.), North Holland Amsterdam, pp. 207-220.
- Rudnicki, J.W. and Rice, J.R. (1975), "Conditions for the localization of deformation in pressure-sensitive dilatant materials", *J. Mech. Phys. Solid.*, **23**(6), 371-394.
- Yao, Y.P., Hou, W. and Zhou, A.N. (2009), "UH model: three-dimensional unified hardening model for overconsolidated clays", *Geotechnique*, **59**(5), 451-469.
- Yao, Y.P., Gao, Z.W., Zhao, J.D. and Wan, Z. (2012), "Modified UH Model: Constitutive modeling of overconsolidated clays based on a parabolic Hvorslev Envelope", *J. Geotech. Geoenviron. Eng., ASCE*, **138**(7), 860-868.
- Zhang, H.W. and Schrefler, B.A. (2001), "Uniqueness and localization analysis of elastic-plastic saturated porous media", *Int. J. Numer. Anal. Method. Geomech.*, **25**(1), 29-48.

JS

## Appendix

The elasto-plastic constitutive tensor of the UH model (Yao *et al.*, 2009) is written as

$$D_{ijkl} = L\delta_{ij}\delta_{kl} + G(\delta_{ik}\delta_{jl} + \delta_{il}\delta_{jk}) - \left( L\frac{\partial f}{\partial \tilde{\sigma}_{mm}}\delta_{ij} + 2G\frac{\partial f}{\partial \tilde{\sigma}_{ij}} \right) \left( L\frac{\partial f}{\partial \tilde{\sigma}_{nn}}\delta_{kl} + 2G\frac{\partial f}{\partial \tilde{\sigma}_{kl}} \right) / X \quad (A1)$$

where

$$\left. \begin{aligned} X &= \frac{\partial f}{\partial \tilde{\sigma}_{ii}} + L\frac{\partial f}{\partial \sigma_{ii}}\frac{\partial f}{\partial \tilde{\sigma}_{jj}} + 2G\frac{\partial f}{\partial \sigma_{ij}}\frac{\partial f}{\partial \tilde{\sigma}_{ij}} \\ G &= \frac{3(1-2\nu)(1+e_0)}{2(1+\nu)\kappa} p \\ L &= \frac{(1+e_0)}{\kappa} p - \frac{2}{3} G \\ \frac{\partial f}{\partial \tilde{\sigma}_{ij}} &= \frac{\lambda - \kappa}{1+e_0} \left[ \frac{M^2 \tilde{p}^2 - \tilde{q}^2}{M^2 \tilde{p}^2 + \tilde{q}^2} \frac{\delta_{ij}}{3\tilde{p}} + \frac{3(\tilde{\sigma}_{ij} - \tilde{p}\delta_{ij})}{M^2 \tilde{p}^2 + \tilde{q}^2} \right] \\ \frac{\partial f}{\partial \sigma_{ij}} &= \frac{\partial f}{\partial \tilde{\sigma}_{kl}} \frac{\partial \tilde{\sigma}_{kl}}{\partial \sigma_{ij}} \\ \frac{\partial \tilde{\sigma}_{kl}}{\partial \sigma_{ij}} &= \frac{1}{3} \delta_{ij}\delta_{kl} + \left( \delta_{ik}\delta_{jl} - \frac{1}{3} \delta_{ij}\delta_{kl} - \frac{s_{kl}s_{ij}}{\ell_\theta^2} \right) \frac{\ell_0}{\ell_\theta} + \frac{s_{kl}}{\ell_\theta} \frac{\partial \ell_0}{\partial I_m} \frac{\partial I_m}{\partial \sigma_{ij}} \end{aligned} \right\} \quad (A2)$$

with

$$\left. \begin{aligned}
 \ell_\theta &= \sqrt{s_{ij}s_{ij}} \\
 \ell_0 &= \sqrt{\frac{2}{3} \frac{2I_1}{3E-1}} \\
 \frac{\partial \ell_0}{\partial I_1} &= \sqrt{\frac{2}{3} \left( \frac{2}{3E-1} + FI_2I_3 \right)} \\
 \frac{\partial \ell_0}{\partial I_2} &= \sqrt{\frac{2}{3}} FI_1I_3 \\
 \frac{\partial \ell_0}{\partial I_3} &= -\sqrt{\frac{2}{3}} FI_1I_2 \\
 F &= \frac{24}{E} \frac{I_1}{(3E-1)^2 (I_1I_2 - 9I_3)^2} \\
 E &= \sqrt{\frac{I_1I_2 - I_3}{I_1I_2 - 9I_3}}
 \end{aligned} \right\} \quad (A3)$$

in which  $L$  and  $G$  are Lamé's constants,  $p$  is the mean principal stress,  $\nu$  is Poisson's ratio,  $I_1$ ,  $I_2$  and  $I_3$  are the first, second and third stress invariants, respectively, and  $s_{kl}$  is the deviatoric stress tensor.  $\tilde{\sigma}_{ij}$  is a transformed stress tensor based on the Matsuoka-Nakai's criterion (1974), and  $\tilde{p}$  and  $\tilde{q}$  are the mean and deviatoric stresses in the transformed stress space. For details of the transformed stress, see Matsuoka *et al.* (1999).